Supplementary Fig. 1. Zhao, et al.

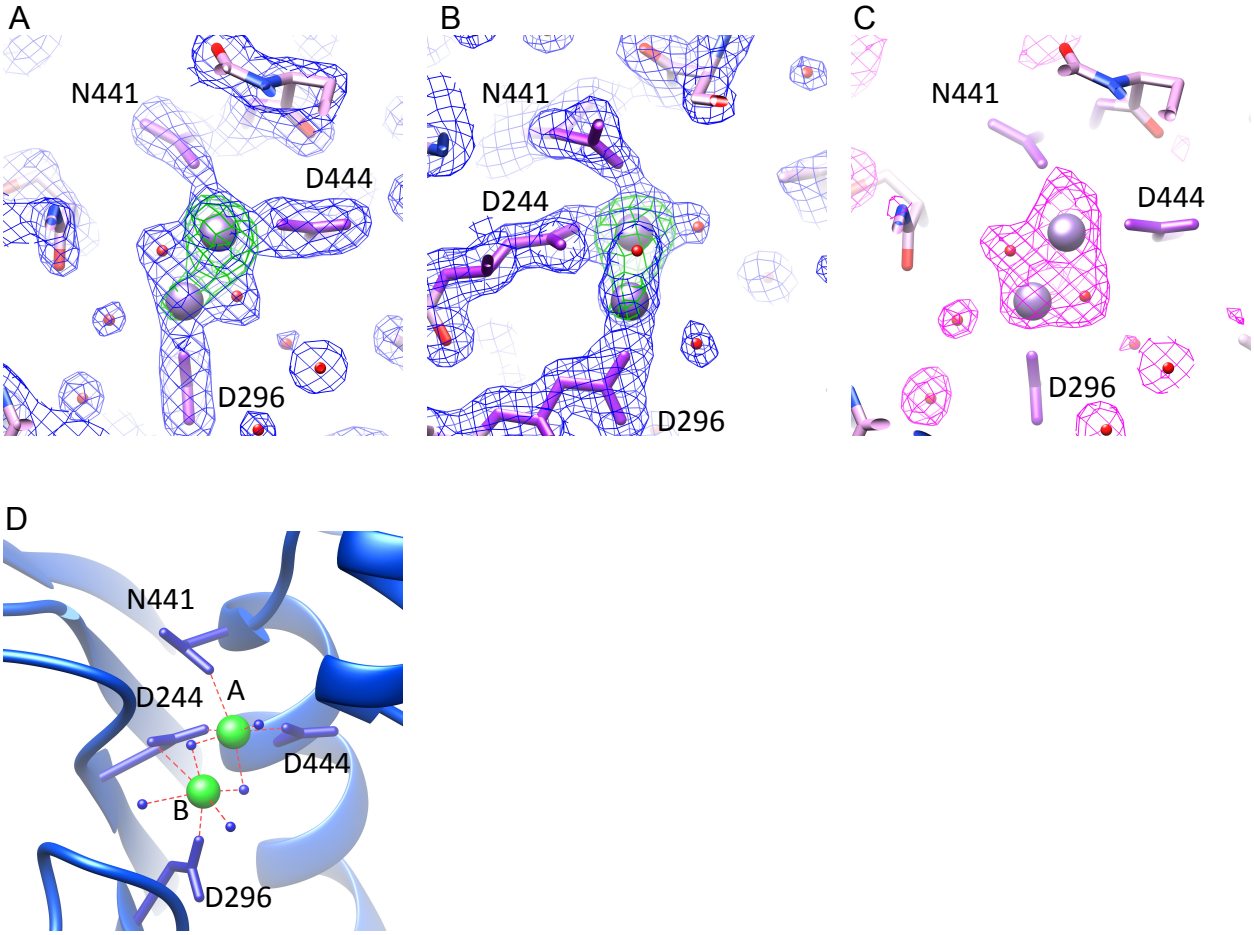

Supplementary Fig. 1. The structures of the gp2C-K428A:Mn^{2+}.
(A) The 1.57 Å resolution 2mFo-DFc electron density map of gp2C:Mn^{2+} (blue mesh) superimposed with the refined model and the anomalous difference map (green mesh) contoured at 1.5 and 8.0 sigma above background repsectively. Water molecules, spheres in magenta. The view is the same as in Fig. 3 A.
(B) A view 90° from (A) about the vertical axis.
(C) The mFo-DFc difference map (magenta mesh) prior to addition of water and metal ions into the model for refinement. The map is contoured at 2.8 sigma above background. The final refined structure (shown as stick model) is superimposed.
(D) the local structure of the active site of gp2C-K428A:Mn^{2+}. The view is identical to that of Fig. 3 D.

Supplementary Fig. 2. Zhao, et al.

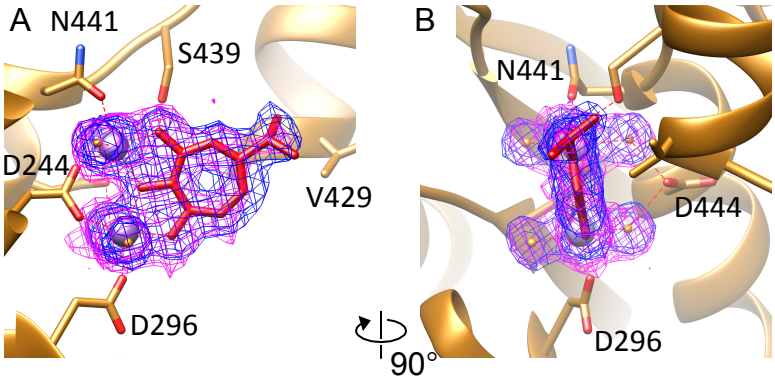

Supplementary Fig. 2. The electron density map of gp2C-K428A:Mn^{2+}:BTP. (A and B) The gp2C-K428A:Mn^{2+}:BTP structure (ribbon diagram in gold) superimposed with the 1.86 Å resolution 2mFo-DFc electron density map contoured at 1.0 sigma (blue mesh) and the mFo-DFc difference map prior to addition of solvent and BTP into the model for refinement contoured at 6.1 sigma (magenta mesh). Side chains of the active site residues as well as S439 and V429 are shown as stick models. BTP, red stick model. The two Mn^{2+}, purple spheres. The four coordinating water molecules, gold spheres.

Supplementary Fig. 3. Zhao, et al.

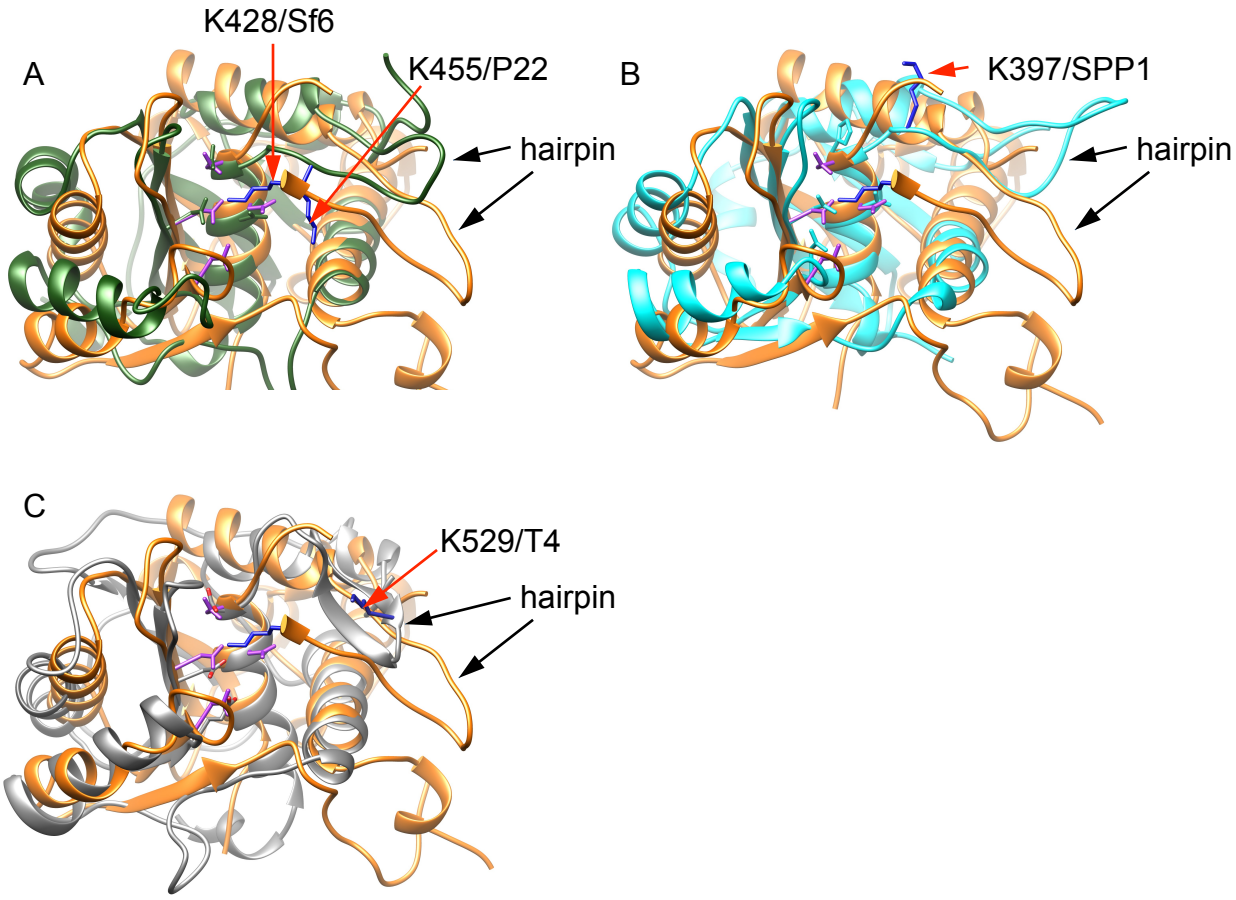

Supplementary Fig. 3. The Sf6 wild-type gp2C structure (gold) was superimposed with those of phages P22 gp2 (green), SPP1 G2P (cyan) and T4 gp17 (metallic) in (A), (B) and (C) respectively. The lysine residues in P22 and SPP1 TerL proteins that occupy a position similar to Sf6 gp2C K428 are shown as stick models in blue. The lysine residue K529 in T4 TerL is shown as a stick model. Acidic residues in the active sites are shown as stick models. Residues 429-435 in Sf6 gp2C were removed in the figures for clarity. Note that those lysine residues are located on similar hairpin structures (black arrows) in those TerL proteins, and their distances from the active site appear to coincide with those of the hairpin structures.

Supplementary Fig. 4. Zhao, et al.

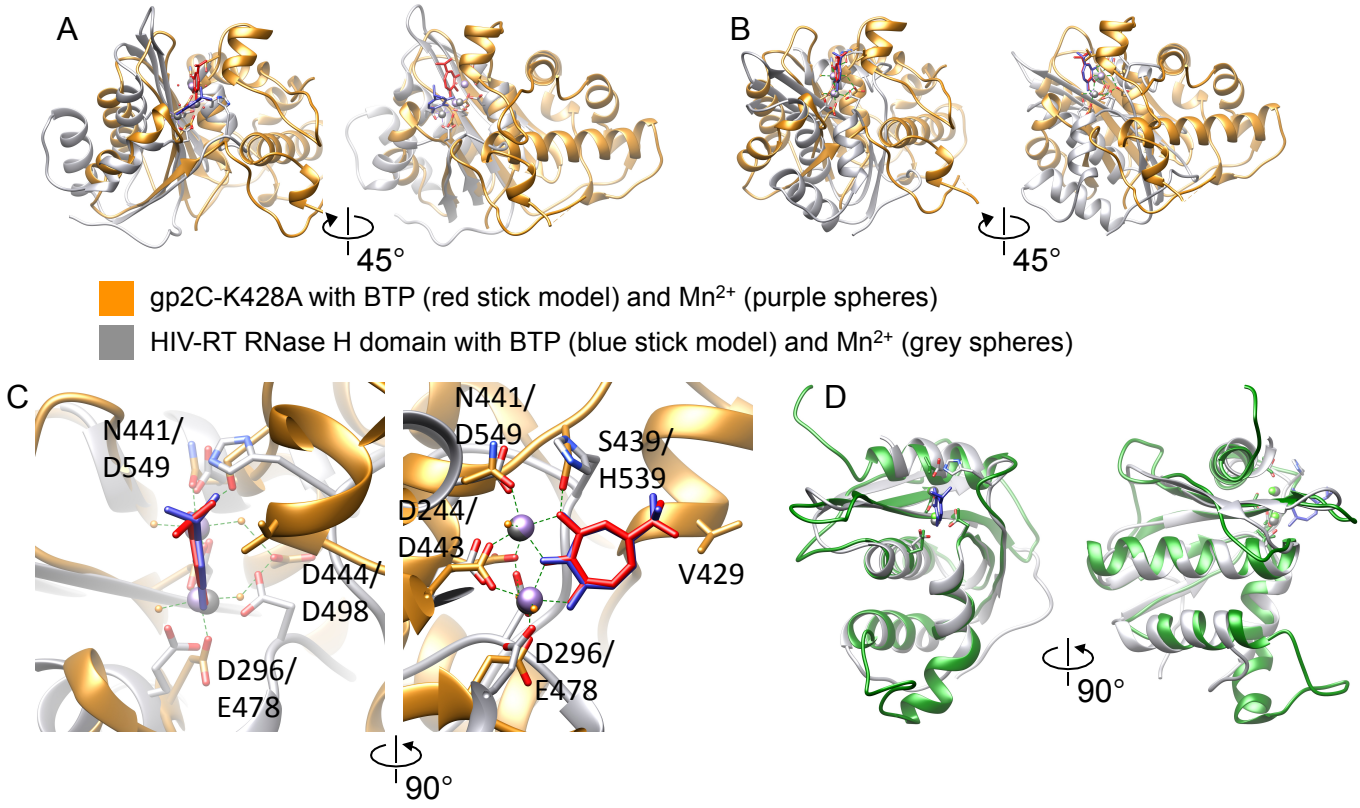

Supplementary Fig. 4. Structural comparison of gp2C-K428A:Mn^{2+}:BTP, HIV-RT RNase H domain in complex with BTP (RCSB PDB code 3IG1) and human RNase H1 in complex with an RNA/DNA hybrid and Ca^{2+} (RCSB PDB code 2G8H).
(A) The gp2C-K428A:Mn^{2+}:BTP structure (gold) is superimposed onto HIV-RT RNase H (grey) according to the common folds, showing remarkably different locations of bound Mn^{2+} and BTP. Side chains of active side residues are shown as stick models.
(B) The Mn^{2+} and BTP substructure of gp2C-K428A:Mn^{2+}:BTP (gold) is superimposed onto that of HIV-RT RNase H (grey). Notice that the folds of the two proteins are no longer superimposed with each other.
(C) Closeup of the active site local structures after superimposition in (B). Coordination bonds of the two metal ions are shown as green dashed lines. Notice that active side residues D443, D549 and E478 of HIV-RT superimpose well with D244, N441 and D296 of gp2C respectively, and that the fourth active site residue D498 of HIV-RT also occupies a position similar to that of D444 in gp2C. Each superimposable pair of active site residues are indicated with the residue numbers in gp2C on the top and in HIV-RT on the bottom respectively.
(D) Superimposition of HIV-RT RNase H domain (grey) with human RNase H1 (green), with an rms deviation of 0.923 Å for 68 Cα atoms. The two Ca^{2+} ions in RNase H1 are shown as green spheres.